A Precoding and Power Control Scheme for SAR Reduction in Indoor MIMO Multicarrier Systems

PAT CHAMBERS[1], (Member, IEEE), AND **TIM W. C. BROWN**[2], (Member, IEEE)
[1]engCORE, Institute of Technology Carlow, Carlow, R93 V960 Ireland
[2]5G/6G Innovation Centre, Institute for Communication Systems, University of Surrey, Guildford, GU2 7XH, U.K.

Corresponding author: Pat Chambers (chambersp@itcarlow.ie)

ABSTRACT In this work, a novel strategy for lowering the uplink user exposure index (EI) is described for an indoor narrowband use-case. This metric measures the long term exposure to electromagnetic radiation a user receives from a device operating in the uplink from the user terminal to the access point. The specific type of device chosen for the exposition of this novel method was a laptop computer and results presented herein specifically target an aspect of this metric called the specific absorption rate (SAR). It is firstly shown that SAR, in the context of a laptop, may be modeled in a similar fashion to the more familiar smartphone analyses that appear in literature. Secondly, an algorithm comprising a mixture of precoding and power control is proposed for usage in the uplink where it is seen to reduce uplink user EI. This proposed approach can provide a reduction in the long-term exposure of the user or be used as a means to increase the transmit power of the device while maintaining SAR compliance. It is shown that if quality-of-service (QoS) is maintained, the proposed approach can achieve a median reduction in SAR of 50 %, which in turn is seen to lower the EI by 30 %. Furthermore, a 60 % median reduction in SAR may also be possible if a minor degree of decrease in QoS is tolerated, which in turn is seen to lead to a 50 % reduction in the EI.

INDEX TERMS Electromagnetic exposure reduction, exposure index, LTE, multi-carrier, MIMO, OFDM, SAR reduction.

I. INTRODUCTION

Electromagnetic (EM) exposure reduction strategies for next generation wireless transmitters must now be considered due to the risk adverse health effects associated with EM radiation that have recently been described [1], [2]. Laptops, smart phones and tablets are all devices that are placed close to the body and must transmit EM radiation in order to perform their associated tasks. Currently, strict regulations for the permissible specific absorption rate (SAR) levels from electronic devices have been set by both the Federal Communications Commission (FCC) [3] and the Comité Européen de Normalisation Electrotechnique (CENELEC) [4]. The SAR metric addresses short-term exposure effects such as tissue heating. However more recently, it has emerged that exposure to EM radiation may have more long-term effects, such as the promotion of tumor-growth [5], and as a result of this, it is becoming necessary to examine SAR and its reduction in a more long-term context. Furthermore, in a very recent survey

The associate editor coordinating the review of this manuscript and approving it for publication was Bong Jun David Choi.

paper on exposure reduction [6], it has been stressed that exposure reduction is now highly likely to be incorporated into standardization efforts in 5G and beyond.

Some of the current effort in reducing EM exposure has focused on optimization of scheduling algorithms [5], [7] [8]. Essentially, these algorithms, which operate on a system level, seek to transmit a certain payload of bits to a given user over a certain time-slot duration. They reduce exposure by re-engineering the bit transmission with a more power efficient emphasis. The focus here is on a link level solution to reducing the SAR in the digital baseband domain for the use case of an indoor laptop operating in a narrowband channel. This clearly could be used in conjunction with system level approaches since reductions in SAR would further scale these scheduling efforts. Other efforts to reduce exposure have focused on antenna design. In their efforts to design smart antennas for SAR reduction in [9], [10], they first characterized SAR in terms of its behavior when a phase offset copy of a signal was simultaneously transmitted with its original by using one radio frequency (RF) chain and a phase splitter. In related work on smart antenna arrays, [11]

suggested that mutual coupling (MC) is unwanted from the perspective of reducing SAR due to its ability to limit the antenna directionality. In [12], F-shaped stubs were shown to significantly reduce coupling and [13], [14] examined how meta-material slabs can reduce MC over a large bandwidth. Furthermore [15] describes how high isolation diplexers may be constructed to reduce MC by carefully engineering circular slots between resonating elements. In [16], lowered MC over large bandwidths using defected ground structures was also described.

It is proposed here to address exposure reduction by examining signal-processing techniques specifically for multiple-input/multiple-output (MIMO) systems. Trade-offs made in the design of MIMO techniques have traditionally been analyzed in terms of trading off data throughput levels for link reliability, i.e., the 'diversity-multiplexing' trade-off [17]. Latterly, power consumption has also been introduced as a third performance trade-off in signal-processing design [18], [19], however in this work, signal-processing for SAR reduction will be considered as another possible system performance trade-off. Using MIMO signal-processing in the baseband digital domain to reduce SAR is a relatively new field of research. In [20], two system models were developed where one used transmit (Tx) channel state information (CSI) to perform beamforming at the receiver and the other, which did not have Tx CSI, but was able to be 'SAR aware', i.e., could exploit knowledge of SAR in order to boost Tx power but stay in SAR limits. A beamforming approach based on Tx CSI approach was then further developed in [21] where a dual information theoretical optimal and SAR reduction precoder was proposed. Using a rigorous mathematical analysis, it was shown that the waterfilling of singular value decomposition (SVD) based eigenmodes could be altered to make the dual accommodation of maximized data throughput and SAR reduction by implementing a precoder based on the SVD itself in conjunction with other precoder structures similar to the ones used in MIMO systems operating in spatially correlated channels. While the work was groundbreaking from an information theory point-of-view, it may exhibit impracticalities due to the fact that waterfilling is required, which in turn requires very accurate Tx CSI as well as increased system complexity. In relation to this, a similar algorithm and precoder approach has also been offered in recent work in [22]. While the work is notable, it is not directly comparable to what is offered here since energy efficiency is being improved with respect to a fixed SAR constraint rather than an explicit SAR reduction. In [23], [24], 'SAR codes' were described, which are an attempt to form a null at the user by transmitting standard modulation symbols from one Tx antenna while transmitting a phase offset of these modulation symbols from another Tx antenna. The premise here is that given a SAR aware phase offset θ_{SAR}, separate information could be encoded into the second Tx antenna stream with respect to the first by virtue of using either $\pm\theta_{\text{SAR}}$ as the phase offset. However, there are issues with this approach, namely: (i) it would violate the linearity condition
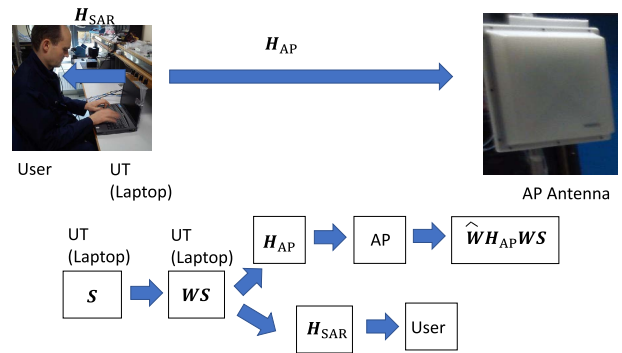

FIGURE 1. System model in both illustrated (above) and block diagram (below) forms. The precoder matrix W operates on the multi-carrier signal S before being transmitted through the channel between the UT and the user's body H_{SAR} and through the uplink channel between the UT and the AP H_{AP}. At the AP, the matched filter $\widehat{W}$ is then applied.

of the Fourier transform, thus making it impractical for use in orthogonal frequency division multiplexing (OFDM); (ii) the reliance on θ_{SAR} to design modulation symbols may lead to impractical modulation alphabets and (iii) while the approach allows for multi-stream transmission, the streams are not truly independent of one another leading to less data being transmitted.

The main contributions of this work are:

1) To show how multi-user MIMO precoding can be redesigned to incorporate a model for SAR and thus expand on previous efforts to incorporate SAR modeling into system design in literature [9], [10].
2) To show how a novel combination of appropriate MIMO precoding design and power control (PC) can be used to reduce SAR and hence effect a reduction in the uplink EI but also facilitate true multi-stream transmission while also maintaining quality of service (QoS) at the access point (AP).
3) To provide a novel far-field analysis and modeling of SAR that examines the applicability of the near-field SAR models in literature [9], [10] [20] to the far-field case.

This paper is organized as follows. In Section II, the system model for SAR reduction using precoding and power control is proposed. Appropriate measurements are described in Section III. In Section IV, the aforementioned far-field SAR model is presented while in Section V the design of the novel precoder, first introduced in Section II, will be described in terms of channel measurements. In Section VI, channel measurement based results of SAR reduction and QoS at the AP are presented and some concluding remarks are given in Section VII.

II. SYSTEM MODEL

As depicted in Fig. 1, there are two MIMO channels, one between the user terminal (UT) and the AP, assigned: $\mathbf{H}_{\text{AP}}$ and of dimension $N_{\text{Rx}} \times N_{\text{Tx}}$, and another between the UT and user themselves, assigned $\mathbf{H}_{\text{SAR}}$ and of dimension

$N_{\text{Rx}} \times N_{\text{Tx}}$. It should be stressed here that N_{Rx} and N_{Tx} vary in this work according to context and that this will be made clear in each case. As will be seen in Section III, $\mathbf{H}_{\text{AP}}$ is subject to the usual assumptions regarding stationarity and fading while $\mathbf{H}_{\text{SAR}}$ is assumed to be more static and will be shown later to be possible to model statistically from channel measurements. In Section V, the leakage based precoder in [25], which was originally designed to allow for multi-user MIMO communications, will be redesigned appropriately to provide SAR reduction. A feature of this particular precoder is that, unlike many linear precoders for multi-user systems, i.e., zero-forcing (ZF), minimum mean square error (MMSE), block diagonalization (BD), etc [26], [27], this design does not require that the number of Tx antennas be greater than or equal to the total number of receive (Rx) antennas. The desire here is to reduce the power to a series of antennas placed on the body's chest cavity while maintaining the same power level at the AP. This is in fact analogous to users having many Rx antennas being served only a limited number of Tx antennas, hence the choice of the design in [25] over the others. Also, similar to multi-user context in [25], it will be assumed that the AP has knowledge of the channel $\mathbf{H}_{\text{AP}}$, which is updated on a frame-by-frame basis and is assumed to remain constant over the frame. The AP is also able to feedback channel weights that are computed based on this channel knowledge. The AP also has statistical knowledge of the channel $\mathbf{H}_{\text{SAR}}$, which will be discussed in more detail in Section V. In Fig. 1, it can be seen that a matrix $\mathbf{S}$ appears on the far left. This $N_{\text{Tx}} \times N_S$ matrix contains the independent multi-carrier transmit data streams and may be defined for the specific case of two transmitters ($N_{\text{Tx}} = 2$):

$$\mathbf{S} = \begin{bmatrix} s_{1,1} & s_{1,2} & s_{1,3} & \cdots & s_{1,N_S} \\ s_{2,1} & s_{2,2} & s_{2,3} & \cdots & s_{2,N_S} \end{bmatrix}. \tag{1}$$

Each row of $\mathbf{S}$ corresponds to a Tx output frame and each column a sampling interval. $s_{1,n}$ and $s_{2,n}$ refer to two Tx symbols emitted from two Tx antennas within one sampling period and N_S is the total number of samples per transmit frame. It is assumed that these two symbol-streams have some form of MIMO and multi-carrier signal processing applied to them. Here, the long term evolution (LTE) standard that uses the space-frequency block code structure was in fact implemented in $\mathbf{S}$ however it should be stressed that any MIMO multi-carrier signal structure may be combined with the precoding approach proposed in this work. Consider now the following $N_{\text{Tx}} \times 1$ precoder vector $\mathbf{w}$ defined as:

$$\mathbf{w} = v_{\max}\left\{\mathbf{B}^{-1}\mathbf{A}\right\}, \tag{2}$$

where:

$$\mathbf{A} = \mathbf{H}_{\text{AP}}^H \mathbf{H}_{\text{AP}}, \tag{3}$$

$$\mathbf{B} = \mathbf{H}_{\text{SAR}}^H \mathbf{H}_{\text{SAR}}. \tag{4}$$

The matrices $\mathbf{A}$ and $\mathbf{B}$ are both square matrices of dimension $N_{\text{Rx}} \times N_{\text{Tx}}$ and the notation, $v_{\max}(\cdot)$ refers to the maximum

eigenvector of its matrix argument and $(\cdot)^H$ refers to the conjugate transpose. To the right of $\mathbf{S}$ in Fig. 1, the precoder matrix $\mathbf{W}$ appears where its columns, i.e., $\mathbf{w}$, are scaled by: $\frac{1}{\sqrt{2}\|\mathbf{w}\|}$, which for the case of $N_{\text{Tx}} = 2$ transmit antennas and $N_D = 2$ data streams satisfies $\|\mathbf{w}\|^2 + \|\mathbf{w}\|^2 = 1$. It should be stressed here that while $N_{\text{Tx}} = N_D = 2$ throughout, it is necessary to distinguish these terms, not least in relation to $\mathbf{W}$. Next, the $N_{\text{Tx}} \times N_D$ precoding matrix $\mathbf{W}$ is then applied to $\mathbf{S}$ to form precoded transmit data streams in the $N_{\text{Tx}} \times N_S$ matrix $\mathbf{X}$ as:

$$\mathbf{X} = \mathbf{WS}. \tag{5}$$

This in turn means that the AP sees a $N_{\text{Tx}} \times N_S$ receive signal $\mathbf{Y}$, which may be written as:

$$\mathbf{Y} = \mathbf{H}_{\text{AP}}\mathbf{X} + \mathbf{n} \tag{6}$$

$$= \mathbf{H}_{\text{AP}}\mathbf{WS} + \mathbf{n}, \tag{7}$$

where $\mathbf{n}$ is an $N_{\text{Rx}} \times 1$ vector of added white Gaussian (AWGN) noise samples with zero mean and identity covariance matrix, i.e., $\mathbf{n} \sim \mathcal{CN}(0, \mathbf{I})$. Finally, at the AP receiver, a matched filter of the form:

$$\widehat{\mathbf{W}} = \frac{\mathbf{W}^H \mathbf{H}_{\text{AP}}^H}{\|\mathbf{WH}_{\text{AP}}\|_F^2}, \tag{8}$$

is applied to $\mathbf{Y}$. Thus, the overall aim of $\mathbf{W}$ is to reduce the signal energy that propagates through the channel $\mathbf{H}_{\text{SAR}}$ to the user's body at the UT without adversely affecting the SNR at the AP.

Consider now the Rayleigh-Ritz quotient (RRQ) result [25]:

$$\max\left\{\frac{\mathbf{W}^H \mathbf{AW}}{\mathbf{W}^H \mathbf{BW}}\right\} = \lambda_{\max}\left\{\mathbf{B}^{-1}\mathbf{A}\right\}, \tag{9}$$

where $\lambda_{\max}\{\cdot\}$ refers to the maximum eigenvalue of its matrix argument. This equation holds if $\mathbf{B}$ is invertible. The term on the left hand-side is in fact the RRQ and its behavior is such that, as indicated, it will maximize the ratio of $\frac{\mathbf{W}^H \mathbf{AW}}{\mathbf{W}^H \mathbf{BW}}$ when the maximum eigenvector of $\mathbf{B}^{-1}\mathbf{A}$ is applied appropriately. It is this fact that provides the reduction in SAR because numerically, the term $\mathbf{W}^H \mathbf{BW}$ is much reduced by comparison to the term $\|\mathbf{B}\|_F^2$, which is in fact a measure of SAR at the UT. However an issue with the RRQ is that often it will reduce the term $\mathbf{W}^H \mathbf{AW}$ by comparison to $\|\mathbf{A}\|_F^2$. While this reduction is less severe than in the case of $\|\mathbf{B}\|_F^2$, it does in fact amount to a reduction in the gain at the AP. Thus, in order to palliate this effect, a simple PC algorithm is now introduced. $\mathbf{H}_{\text{AP}}$ is used to compute the power gain of the AP channel, i.e., $\|\mathbf{H}_{\text{AP}}\|_F^2$ in line 1. Similarly when the precoder $\mathbf{W}$ is applied, the appropriate AP channel gain is computed as: $\|\mathbf{H}_{\text{AP}}\mathbf{W}\|_F^2$ in line 2. The if-conditional on line 3 simply compares these two power gains and if there is a reduction in the power gain at the AP, a scale factor γ is subsequently computed. This is in turn used to scale $\mathbf{W}$ on line 8. The overall aim of the PC algorithm is to compute γ in order to maintain QoS at the AP while also providing a reduction in SAR. Further to this,

---

Algorithm 1 PC Algorithm

Inputs: $\mathbf{H}_{AP}$, $\mathbf{W}$.
Output: $\mathbf{W}$.

1: $G_{AP} \leftarrow \|\mathbf{H}_{AP}\|_F^2$
2: $G_{SAR} \leftarrow \|\mathbf{H}_{AP}\mathbf{W}\|_F^2$
3: **if** $G_{SAR} < G_{AP}$ **then**
4:     $\gamma \leftarrow \sqrt{\dfrac{G_{AP}}{G_{SAR}}}$
5: **else**
6:     $\gamma \leftarrow 1$
7: **end if**
8: $\mathbf{W} \leftarrow \gamma \mathbf{W}$
9: $G'_{SAR} \leftarrow \|\mathbf{H}_{SAR}\mathbf{W}\|_F^2$
10: $G''_{SAR} \leftarrow \|\mathbf{H}_{SAR}\|_F^2$
11: **if** $G'_{SAR} > G''_{SAR}$ **then**
12:     $\gamma \leftarrow 1 - \sqrt{\dfrac{G'_{SAR}}{G''_{SAR}}}$
13:     $\mathbf{W} \leftarrow \gamma \mathbf{W}$
14: **end if**

---

lines 9 - 14 act as a fail-safe to stop the SAR ever increasing beyond whatever it would have been had this scheme not been applied. This fail-safe however was never triggered by the measurements in this work. One final detail here is that the precoder $\mathbf{W}$ requires knowledge of $\mathbf{H}_{AP}$ and $\mathbf{H}_{SAR}$ to undertake this function. Precoder design that incorporates sensible decisions about the update rate of channel knowledge for $\mathbf{H}_{AP}$ and also incorporates SAR awareness for $\mathbf{H}_{SAR}$ will thus be the subject of Section V.

III. CHANNEL MEASUREMENTS

The goal of the work is to develop a novel system model based on the redesign of multi-user precoding to reduce exposure to the user in the far-field. The most logical candidates for this are laptops and tablets. These devices predominantly operate indoors, where the velocity of the device is minimal and the Doppler is dominated by people's movements in the channel. As a result, our experimental design was envisioned to accommodate this. Future work will examine the smartphone scenario, where harsher more wideband channels would be encountered with greater degrees of Doppler effect. Two channel measurement campaigns are now described. The first pertains to SAR modeling and the design of the precoder matrix, $\mathbf{W}$. The second is to assess the precoder and PC performance in terms of SAR reduction and the ability to maintain QoS at the AP. In both cases an Elektrobit Propsound wideband MIMO channel sounder was used and the measurements are partitioned into multidimensional arrays, where bold matrix/vector notation is used throughout when referring to them for convenience. Further to this, the notation $\widehat{\mathbf{H}}_{SAR}(\tau, i, j, t)$ appears twice here, once in Section III-A and once in Section III-B. This refers to SAR measurements under two slightly different contexts. Thus in the sections that follow this one, it will be clearly stipulated which is pertinent.

TABLE 1. Channel sounder parameters.

Parameter	Value
Tx Power	-10 dBm.
No. of transmitters, N_{Tx}	2 (Section III-A)
No. of transmitters, N_{Tx}	4 (Section III-B)
No. of receivers, N_{Rx}	4 (Section III-A)
No. of receivers, N_{Rx}	6 (Section III-B)
No. of measurements per scenario, T	3000
Carrier frequency, f_c	2.3 GHz
Sampling frequency of MIMO array	23.774202 Hz.
System bandwidth	10 MHz.
No. of delay bins, N_b	254

A. SAR MODELING AND PRECODER DESIGN MEASUREMENTS

In Fig. 2 (a), four omnidirectional receive antennas were mounted onto a coat in order to measure the user's far field SAR at the chest cavity. In Fig. 2 (b), a laptop user wears this coat and is in a position to operate the laptop as well as type and make appropriate hand movements, which a person would make when seated at a laptop. The source of transmission, shown in Fig. 2 (c) are four transmit antennas mounted on top of the laptop each positioned at approximately $\frac{\lambda}{2}$ (6 cm), with respect to a carrier frequency f_c of 2.3 GHz, apart. For the SAR modeling in Section IV, these four antennas will comprise three separate pairs of transmit antennas and are the three sets of measurements that will be used to support that analysis. However in the context of precoder design in Section V, only the middle pair will be used to extract the channel between UT and user's body and will form the basis for the design of the component $\mathbf{B}$ of the precoder $\mathbf{W}$. The probe antennas used here were MRM-UMB-3C-BLK-12 ultrawideband antennas (UWB) [28] with a 2.5 dBi gain and before any channel measurements were undertaken with the sounder, their response was examined by using a carefully calibrated rotating surface in an anechoic chamber. Two sets of anechoic chamber measurements were made, one where the antennas were on the body, as in Fig. 2 (d), and another where the antennas were measured in free space using a similar set-up as in Fig. 2 (d) except that the person shown was replaced by the white cylindrical holder. The goal of these two initial sets of measurements was to determine how much of an effect the body and material in the coat would have on the response of the antennas. The experimental results are presented in Fig. 3. Since the human body must rotate with the antenna, anything in the angular range outside of -50^0 to $+50^0$ can be ignored and the remaining valid comparison within this range shows little effect on antenna gain whether the antennas be in free space or on-body. Thus, these antennas are deemed adequate to be on-body probe antennas for SAR measurements.

Having determined that the antennas used as on-body probes are adequate, channel sounding could then be performed with the parameters given in Table 1. The transmit power of -10 dBm was determined by the software in the
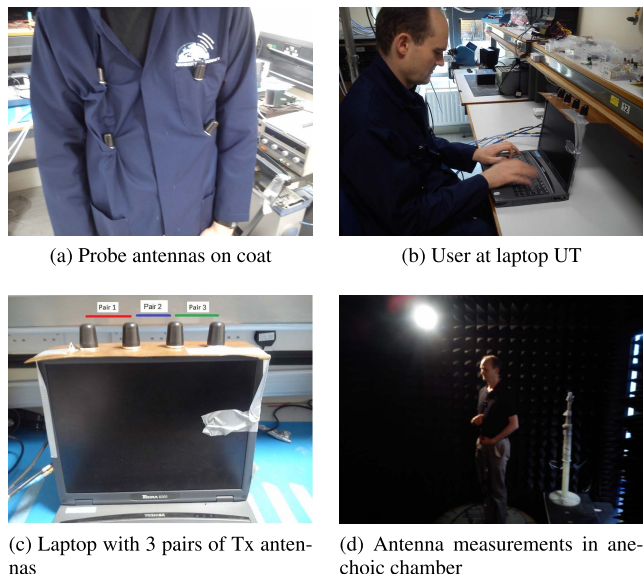
(a) Probe antennas on coat

(b) User at laptop UT

(c) Laptop with 3 pairs of Tx antennas

(d) Antenna measurements in anechoic chamber
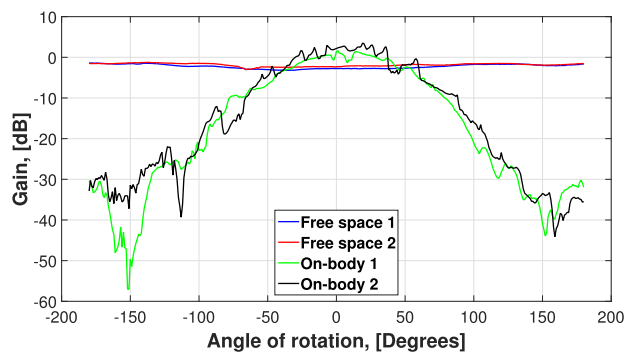
FIGURE 2. Channel measurement equipment.

FIGURE 3. Free space and on-body response of UWB probe antennas.

channel sounder and reflects the desire not to clip or distort the received sounder signal as measured on-body. The total number of transmitters N_{Tx} is logically four and the total number of receive antennas N_{Rx} is also four, given the previously mentioned probe antennas. The channels are measured at a carrier frequency f_c of 2.3 GHz, which reflects the need to analyze the popular ISM band Wi-Fi frequency of 2.45 GHz without measuring interference. The sampling frequency of the entire MIMO array was 23.774202 Hz, which would be well within acceptable limits given what degree of Doppler effect would be experienced in an indoor pedestrian scenario. The sounder uses a correlative procedure in conjunction with transmit pseudo-binary sequences thus allowing for an accurate measurement of all aspects of the MIMO spatial channel. The system bandwidth was 10 MHz and this was chosen because much of the analysis will be underpinned by the 10 MHz long term evolution (LTE) MIMO-OFDM standard. Finally, since the correlative procedure that the channel sounder uses to obtain the channel impulse response (CIR) imposes a $sinc^2$ function mask on the frequency domain of the channel measurements, an inverse $sinc^2$ function, whose maximum value was constrained to

TABLE 2. Six campaign scenarios.

Scenario	Description
1	Channel from sounder Tx 1 to Sounder Rx. No people in channel.
2	Channel from sounder Tx 1 to Sounder Rx. People walking in channel.
3	Channel from sounder Tx 2 to Sounder Rx. No people in channel.
4	Channel from sounder Tx 2 to Sounder Rx. People walking in channel.
5	Channel from sounder Tx 3 to Sounder Rx. No people in channel.
6	Channel from sounder Tx 3 to Sounder Rx. People walking in channel.

unity, was applied in post-processing to all of the channel measurements conducted. The result of all this is a four dimensional array: $\widehat{\mathbf{H}}_{SAR}(\tau, i, j, t)$, which is a function of CIR component (per bin) τ, Rx element number i, Tx element number j and measurement at a given time t with a total of 3000 measurements being made.

B. SYSTEM PERFORMANCE MEASUREMENTS

In this case, careful examination of the photos in Fig. 2 reveals that a total of 24 MIMO channels were measured in a 6×4 configuration. The receivers were again comprised of the four probe channels but now with an additional two channels at the AP to make six. In order to introduce repeatability into the AP measurements, the user and laptop were positioned at three different points in a partitioned room with doorways as shown in the floor plan diagram in Fig. 4. In Fig. 5, photos of these three positions from the point of view of the AP are shown. The labels: Sounder Tx 1, Sounder Tx 2 and Sounder Tx 3, refer to the positions of the laptop while Sounder Rx refers to the AP. At each of the three Tx positions, two campaigns were undertaken (thus a total of six campaigns in total), one with some people moving in the channel between the Tx (UT) and the Rx (AP) and another with no people in that channel. These are summarized in Table 2. It should be stressed at this point that while the system model in Section II stipulates $N_{Tx} = 2$, the use of $N_{Tx} = 4$ in Table 1 refers to the sounding of three transmit antenna pairs for the sake of experimental repeatability. All of the other sounding parameters mentioned in Section III-A remained the same throughout this campaign. Also, similar to Section III-A, the result is a pair of four dimensional arrays $\widehat{\mathbf{H}}_{SAR}(\tau, i, j, t)$ and $\widehat{\mathbf{H}}_{AP}(\tau, i, j, t)$, each containing 3000 measurements in their fourth dimension for each of the six scenarios outlined.

IV. FAR-FIELD SAR MODELLING

Far-field SAR is now calculated from the channel measurements in $\widehat{\mathbf{H}}_{SAR}(\tau, i, j, t)$ from Section III-A. From this, the calculations are compared with a model for SAR that pertains to smartphone channels in the near-field in order to ascertain this model's applicability to the far-field case.
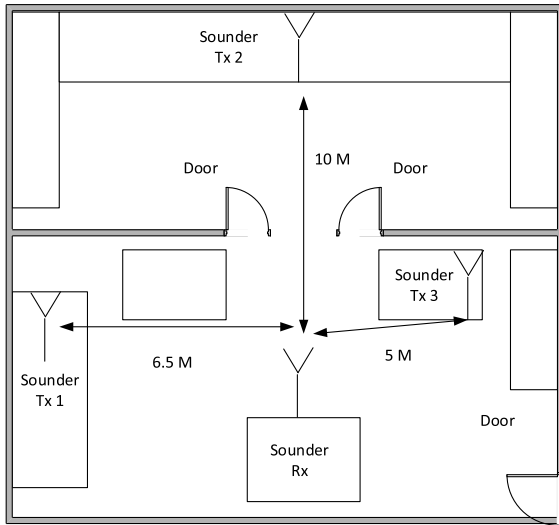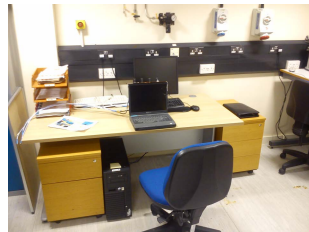
FIGURE 4. Floor plan diagram for three different sets of SAR and AP measurements.
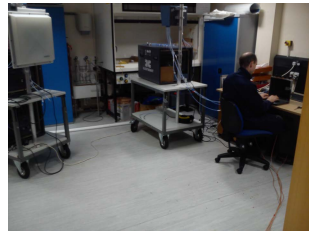

(a) Sounder Tx1 (Laptop with user and probes) viewed from AP

(b) Sounder Tx2 (Laptop with user and probes) viewed from AP

(c) Sounder Tx3 (Laptop with user and probes) viewed from AP

(d) Sounder Rx (AP) while Sounder Tx1 is transmitting

FIGURE 5. Sounder Tx and Rx.

A. SAR CALCULATIONS

It is first necessary calculate the whole body SAR SAR_{wb} of the chest cavity of a laptop user. Much of the calculation framework presented in this section is based on what is outlined in [29]. In their approach, they take the incident power density at the point where the EM wave just enters the body and from this, they can incorporate volume and spatial integration as well as tissue layering effects to arrive at a calculation of SAR. On the basis of a rigorous statistical analysis of SAR measurements in body phantoms, they effectively convert incident power density into whole-body SAR measurements. However, what is different here is that in [29], only a single Tx antenna is considered and a channel model is used to calculate the incident power density at the body based on Tx power levels, while here multiple Tx antennas are considered and the incident power density is based on channel measurements. Thus, the calculations used here may be summarized concisely as follows. To begin, consider that the average incident power $P_{i,t}$ may be calculated from each tth channel measurement in (10), as shown at the bottom of the page. Also, in (10), the colon notation in $\widehat{\mathbf{H}}_{\text{SAR}}(:, i, j, t)$ denotes a vector containing the measured CIR. $N_{\text{Rx}} = 4$ is the number of probe antennas. It should be noted that $P_{i,t}$ is simply a calculation of the power in the MIMO channel between a given Tx pair and the set of probe antennas. Thus, the MIMO power at the AP P_{AP} could also be calculated similarly by setting $N_{\text{Rx}} = 2$ and applying the appropriate CIR $\widehat{\mathbf{H}}_{\text{AP}}(:, i, j, t)$. $\mathbf{X}(:, j)$ is the jth transmit MIMO multi-carrier signal. The term $\exp(j2\pi f_c t_s)$ is a scalar multiplier that models the upconversion of the baseband quantities in $\mathbf{X}(:, j)$ and $\widehat{\mathbf{H}}_{\text{SAR}}(:, i, j, t)$ where $j = \sqrt{-1}$ and t_s is the sampling interval of the signal. The notation $\otimes$ is the vector convolution operation. As a result of this, the new vector that is produced has the variance of its elements calculated by the $\text{Var}[\cdot]$ operator. Dropping the subscript t for convenience, these average receive power calculations, P_i, are converted to incident power density calculations $P_{D,i}$ under the assumption of an isotropic antenna as follows:

$$P_{D,i} = 4\pi \frac{P_i}{\lambda^2}. \tag{11}$$

From this, a quantity known as impinging SAR, $\text{SAR}(0)$, is calculated as:

$$\text{SAR}(0) = \frac{\sigma_i}{\rho} Z_i \, |t_{\text{co}}|^2 \, P_{D,i}, \tag{12}$$

where the transmission coefficient t_{co} is defined:

$$t_{\text{co}} = \frac{2}{1 + \sqrt{\epsilon_r}}, \tag{13}$$

and where σ_i is the conductivity of the medium into which the EM wave is about to impinge and ρ is its density. In both cases, this medium is the human body with σ_i being frequency dependent and derivable from tables in [30] while ρ for the human body is generally accepted to be 1000 kg/m^3. Z_i is the characteristic impedance of the medium in which the EM wave has propagated, i.e., air. The term ϵ_r is the complex relative permittivity and is given by:

$$\epsilon_r = \epsilon_r' - j\left(\frac{\sigma_i}{\epsilon_0 \omega}\right), \tag{14}$$

$$P_{i,t} = \frac{1}{N_{\text{Rx}}} \sum_{i=1}^{N_{\text{Rx}}} \text{Var}\left[\sum_{j=1}^{N_{\text{Tx}}} \Re\left\{\mathbf{X}(:, j) \otimes \widehat{\mathbf{H}}_{\text{SAR}}(:, i, j, t) \exp(j2\pi f_c t_s)\right\}\right] \tag{10}$$

where ϵ'_r is simply the real part of the relative permittivity and is also found in tables in [30]. ϵ_0 is the permittivity of free space, i.e., 8.85×10^{-12} F/m and $\omega = 2\pi f_c$. Given the expression for impinging SAR SAR (0), in order for an accurate calculation of $\mathrm{SAR_{wb}}$ some further quantities are required. Firstly, the decaying behavior of SAR as electromagnetic radiation penetrates the body is modeled by a quantity known as the penetration depth δ which is written as:

$$\delta = \frac{1}{\omega}\left[\left(\frac{\mu_0 \epsilon'_r \epsilon_0}{2} \right) \left(\sqrt{1 + \left(\frac{\sigma_i}{\omega \epsilon'_r \epsilon_0} \right)^2} - 1 \right) \right]^{-1/2}, \quad (15)$$

where the permeability of free space is $\mu_0 = 4\pi \times 10^{-7}$ H/m. There is also 'tissue layering effect' factor T which arises due to the fact that human tissue is not homogeneous in nature and because of this, an enhancement in the SAR levels can take place. This factor has been set at $T = 10^{0.25}$ here [29]. If it is assumed that the laptop Tx antennas illuminate the entire chest cavity then $\mathrm{SAR_{wb}}$ may be calculated from:

$$\mathrm{SAR_{wb}} = \frac{T}{2} \frac{\delta}{D_{\mathrm{body}}} \mathrm{SAR}(0), \quad (16)$$

where $D_{\mathrm{body}} = 0.089$ m, which is the 95th-percentile depth of the body as derived from a statistical analysis of human body cuboid dimensions conducted in [29].

B. COMPARISON TO SMARTPHONE SAR MODELS

In [9], [10] [20], a model for SAR variation with respect to phase-offset between two Tx streams being emitted from a smartphone into a skull phantom was provided analytically as:

$$\mathrm{SAR}_\theta = P\left(s_1 + s_2 \cos(\theta + \phi) \right), \quad (17)$$

where clearly s_1 and s_2 represent an offset and amplitude scale factor respectively while θ is the phase-offset angle between the two Tx streams and ϕ represents a further phase-offset for the model. In order to confirm whether this model is pertinent to the laptop measurements described in Section III-A, the precoder matrix $\mathbf{W}$ will be applied in this section only as:

$$\mathbf{W} = \begin{bmatrix} 1 & 0 \\ 0 & \exp^{j\theta} \end{bmatrix}. \quad (18)$$

Also the matrix $\mathbf{S}$ from (1) will also be altered in this section such that its two rows, i.e., the two Tx streams, are copies of one another. As a result when $\mathbf{W}$ is applied to $\mathbf{S}$, as in (5), the resultant matrix $\mathbf{X}$ contains two rows that are merely phase-offset copies of one another. When these two Tx streams are then convolved with the CIRs between the UT and the user's body in the manner suggested by (10), a value for $\mathrm{SAR_{wb}}$ can then be calculated by following the framework outlined by (10) - (16). The procedure is repeated a further 359 times in order to obtain a 360 values of $\mathrm{SAR_{wb}}$ where the angle θ was incremented each time. The procedure was undertaken for each of the three probe pairs and averaging

TABLE 3. SAR modelling parameters.

Tx pair	Modelling parameters
1	$s_1 = 0.1721$, $s_2 = 0.2674$, $\phi = 0.3\pi$
2	$s_1 = 0.2530$, $s_2 = 0.3819$, $\phi = 0.4\pi$
3	$s_1 = 0.3349$, $s_2 = 0.4659$, $\phi = -0.3\pi$

was performed over the 3000 measurements available. The results are provided in Fig. 6 where, as in [20], the device's transmit power was set at 1 W.

In order to fit models to the results for $\mathrm{SAR_{wb}}$, (17) was compared. In each case, the terms s_1 and s_2 were obtained by systematic inspection of the measurement-based calculations of $\mathrm{SAR_{wb}}$ while values for ϕ were deduced heuristically using a minimum mean squares estimation (MMSE) method. The entire set of modeling parameters s_1, s_2 and ϕ for each of the three Tx pairs is provided in Table 3. In summary, this analysis reveals that the third Tx pair has a different SAR characteristic to the first two pairs. This is directly comparable to the situation in [20] where the SAR modeling effort with the smartphone showed different phone facial configurations could also yield different SAR characteristics. Overall the advantage of this modelling approach from [9], [10] [20] is that it validates the fact that similar sinusoidal SAR behavior may be observed in the far-field however its disadvantage is that the model is sensitive to the aforementioned configurational differences, which can lead to changes in the sinusoidal pattern.

V. PRECODER DESIGN

The precoder $\mathbf{W}$ comprises $\mathbf{A}$ and $\mathbf{B}$, which are in turn based on $\mathbf{H_{AP}}$ and $\mathbf{H_{SAR}}$ respectively. Throughout this work, the $N_{\mathrm{Tx}} \times N_S$ matrix $\mathbf{S}$ will comprise specifically of the 10 MHz LTE MIMO-OFDM signal, which was designed to derive channel state information from pilots that are spaced temporally every 0.2 ms to accommodate the Doppler effect expected from a 500 km/h velocity and spaced in frequency every 45 kHz to accommodate a coherence bandwidth for a 991 ns long CIR (see Ch. 8.2.1 in [31]). Since, the use-case here is an indoor desk-based laptop, it will be argued how these constraints can be relaxed appropriately for the design of $\mathbf{W}$, particularly given that such an update-rate of $\mathbf{W}$ would be prohibitive from a complexity point-of-view under this regime. Also, for the design of $\mathbf{B}$, a new SAR modeling approach will be described that will not be as sensitive to configuration differences as the one in Section IV-B.

A. DESIGN OF A

The people walking in the channel are the main source of Doppler in this use-case and given an average human walking-pace, $v = 1.4$ m/s [32], this in turn implies a Doppler frequency, $f_d = f_c \times (v/c) = 11.43$ Hz that would require a MIMO sampling period $T_d = \frac{1}{2f_d} = 43.7$ ms. Recall that the sounder is sampling the MIMO array at 23.774202 Hz, which corresponds to a sampling period of 43.5 ms. Thus, when the frame is convolved with the CIRs in this MIMO channel, it is temporally adequate to update $\mathbf{W}$ on a frame-by-frame

basis. With regard to the update of **W** in the frequency domain, a decision needs to be made as to whether the 10 MHz LTE signal is narrow-band or wide-band and such a decision must be based on knowledge of the coherence bandwidth of the channel. In peer-review work at 2.6 GHz, the authors in [33] have offered mean coherence bandwidth calculations. In a similar indoor furnished environment to here and utilizing a much larger experimental bandwidth than here (1 GHz), figures have been offered that are as low as 9.220 MHz for a NLOS channels with people and as high as 12.15 MHz for LOS without people. Given also that the 10 MHz LTE MIMO-OFDM signal used in this work is sampled at 15.36 MHz, which is a lower rate than would expected from the Nyquist criterion, because many of the tones are not used in order to facilitate band-limiting of the signal for reduced interference, this means that **W** can be reasonably updated only once across the entire 10 MHz band for its purpose of SAR reduction. Thus, this signal is experiencing a largely narrowband channel in this environment and thus the channel will be treated as such here. The channel matrix, $\mathbf{H}_{AP}$, can therefore be calculated as sum of multipaths along the dimension, τ, whose delays are similar, and lead to a single-tap channel through a largely constructive interference process [34]:

$$\mathbf{H}_{AP}(i, j, t) = \sum_{\tau=1}^{N_b} \widehat{\mathbf{H}}_{AP}(\tau, i, j, t). \tag{19}$$

The dependency of $\mathbf{H}_{AP}$ on t here simply means that it will be evaluated for each MIMO channel measurement as an $N_{Rx} \times N_{Tx}$ channel matrix that ultimately leads to **A**. It should be stressed here that since $\mathbf{H}_{AP}$ is an uplink wireless channel between the user and the access point, it should be subject to the same issues and improvements regarding pilot symbol design and optimization that have been described in very recent work in [35]. Here, previously flawed assumptions about low correlation in neighboring channels and relations between uplink and downlink channels have been challenged in order to leverage significant system performance improvements.

B. DESIGN OF B

The goal of this section is to derive a model from the measurements in $\widehat{\mathbf{H}}_{SAR}$ in order to derive **B** and hence make the precoder **W** SAR aware. Like in Section IV-A, this section will use the channel measurements $\widehat{\mathbf{H}}_{SAR}$ from Section III-A. Since the channel $\mathbf{H}_{SAR}$ exists between UT and the user's body, it could never be evaluated on an ongoing basis. Thus, it is proposed here that $\mathbf{H}_{SAR}$ be evaluated statistically. To begin, consider the idea of calculating $\mathbf{H}_{SAR}(i, j, t)$ by summing along the τth dimension of $\widehat{\mathbf{H}}_{SAR}$ in a manner similar to (19). In this case, the dependency on t means that there can be a total of T channels of dimension $N_{Rx} \times N_{Tx}$ that can now be analyzed. Thus, in order to design **B**, it is proposed here to develop a spatial model for $\mathbf{H}_{SAR}$ that is based on the first order statistics of the single-tap narrow-band channels
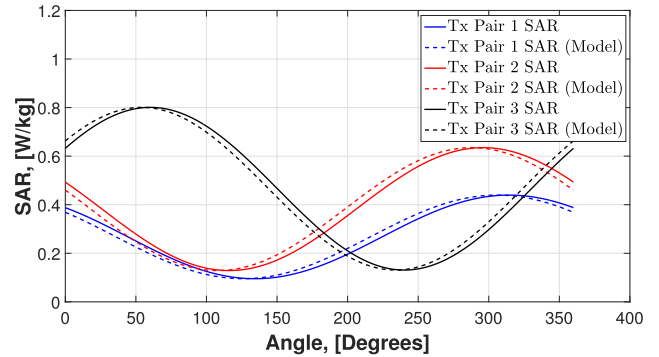

FIGURE 6. Far-field SAR modelling in laptop channels.

in $\mathbf{H}_{SAR}(i, j, t)$ Thus, each set of $N_{Rx} \times N_{Tx}$ channels is normalized with respect to the channel that corresponds to $N_{Rx} = N_{Tx} = 1$. In effect, this model exploits the fact that the overall geometry of the channels between the probes and the middle Tx antenna pair predominates and that any fading caused by hand movements, etc, affects all channels equally. It is also worth noting here that any scaling of **B** (or **A**) will not affect the eigenvectors that are used to define the precoder **W**. In Figs. 7 and 8, a first order statistical analysis in terms of empirically derived cumulative distribution functions (CDFs) of the amplitude and phase respectively of each of the $N_{Rx} \times N_{Tx}$ channels is provided, where the channel $N_{Rx} = N_{Tx} = 1$ has been ommited due to the effect of normalization. These empirical CDFs are then fitted using a maximum likelihood estimation (MLE) technique. The statistical fits in all cases were assumed to be Gaussian, which is reasonable given the highly line-of-sight (LOS) nature of the channel being measured between the UT and the user's body. Any observable deviation from this was assumed to still be close enough to the Gaussian framework to allow for this approach to be used. The details of the shaping parameters μ and σ are tabulated in Table 4 and the mean values, under the μ column, for amplitude and phase are then used to create the channel matrix $\mathbf{H}_{SAR}(i, j)$, which in turn will create the matrix **B** for the precoder **W**. In contrast to the recent improvements in pilot symbol design described in [35], it should be stressed here that for the figures in Table 4, as well as being influenced by the geometry of the channel as mentioned, they are also likely hardware influenced. The channels encountered in this work for the case of $\widehat{\mathbf{H}}_{SAR}$ have been assumed to be narrowband but it may be the case however that for much wider channel bandwidths, as will be encountered in future 5-6G systems, these channels may need to be divided into allocations of 10-20 MHz. Notwithstanding this however, a manufacturer could still determine them accurately by transmitting known signal frames using a testbed and performing a similar analysis to here.

Once $\widehat{\mathbf{H}}_{SAR}$ is evaluated for the case of four probe antennas, it can be evaluated for other configurations of $N_{Rx} \times N_{Tx}$ by removing appropriate rows. **B** is thus evaluated for the cases of four, three and two probe antennas, i.e., as $\mathbf{B}_{42}$, $\mathbf{B}_{32}$ and $\mathbf{B}_{22}$ respectively, using (4) and these remain fixed throughout

TABLE 4. Shaping parameters for PDF curve fits in Figs. 7 & 8.

Fig. 7, curve fit	μ	σ
Gaussian fit, $\mathbf{H}_{SAR}$ (2, 1)	1.3108	0.2379
Gaussian fit, $\mathbf{H}_{SAR}$ (3, 1)	1.7011	0.3009
Gaussian fit, $\mathbf{H}_{SAR}$ (4, 1)	0.5720	0.2214
Gaussian fit, $\mathbf{H}_{SAR}$ (1, 2)	0.9022	0.0883
Gaussian fit, $\mathbf{H}_{SAR}$ (2, 2)	0.9315	0.1736
Gaussian fit, $\mathbf{H}_{SAR}$ (3, 2)	1.7155	0.2639
Gaussian fit, $\mathbf{H}_{SAR}$ (4, 2)	1.0692	0.2467
Fig. 8, curve fit	μ	σ
Gaussian fit, $\mathbf{H}_{SAR}$ (2, 1)	-1.7149	0.2279
Gaussian fit, $\mathbf{H}_{SAR}$ (3, 1)	-3.3173	0.3270
Gaussian fit, $\mathbf{H}_{SAR}$ (4, 1)	-2.3270	0.4040
Gaussian fit, $\mathbf{H}_{SAR}$ (1, 2)	1.4026	0.1444
Gaussian fit, $\mathbf{H}_{SAR}$ (2, 2)	0.3089	0.2352
Gaussian fit, $\mathbf{H}_{SAR}$ (3, 2)	-2.5011	0.3292
Gaussian fit, $\mathbf{H}_{SAR}$ (4, 2)	-1.9947	0.3405

FIGURE 8. Statistical analysis of the phase difference $\theta_{SAR}(i, j)$ of the normalized channels $\mathbf{H}_{SAR}$. The channel $\mathbf{H}_{SAR}(1, 1)$ is omitted due to normalization. Dash-dot lines & circles are used for all channels pertaining to Tx1 while solid lines & squares pertain to Tx2. All fits are Gaussian and the associated shaping parameters are tabulated in Table 4.

A. SAR REDUCTION & AP GAIN

The SAR levels are calculated according to the framework implied by (10) - (16) in Section IV-A. SAR calculations are performed before the precoding and PC algorithm is implemented and the notation SAR_{wb} will be used for these while SAR'_{wb} denotes the SAR calculations after the algorithm's implementation. From this, the quantity ΔSAR may be written:

$$\Delta SAR = 10 \log_{10} \left[\frac{SAR'_{wb}}{SAR_{wb}} \right]. \tag{23}$$

To ascertain the effect on QoS at the AP, the power gain of the precoded MIMO channel between the UT and the AP is calculated according to (6), i.e., by evaluating the output at $\mathbf{Y}$ when the precoder was applied and denoting this as P'_{AP}. This is then compared with the channel gain without the precoder applied and denoted AP Gain to arrive at figure for AP Gain as implied by:

$$AP \text{ Gain} = 10 \log_{10} \left[\frac{P'_{AP}}{P_{AP}} \right]. \tag{24}$$

Throughout, the multi-carrier signal in the matrix, $\mathbf{S}$, that was used was the diversity mode of the 10 MHz LTE MIMO-OFDM communications system derived from the simulators in [36], which uses Alamouti's space-frequency block code (SFBC). However, it should be stressed that this approach can be applied to any multi-carrier MIMO signals (see Section V in [25]) and, indeed, there is also no reason why this system could not be applied to the signal samples of more recent novel non-orthogonal multiple access (NOMA) technologies [37].

In Fig. 9, the CDF of aggregated calculations of ΔSAR over all three Tx pairs and all six scenarios is provided. The four plots evaluate the behavior of Full PC and back-offs of 1 dB, 2 dB, & 3 dB respectively and in each plot, various Rx probe configurations are investigated, i.e., four probe receivers (4×2), three probe receivers (3×2) & two probe receivers (2×2). The role of power back-off is to simply
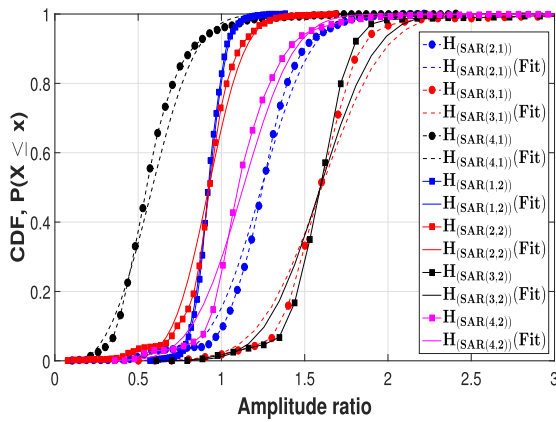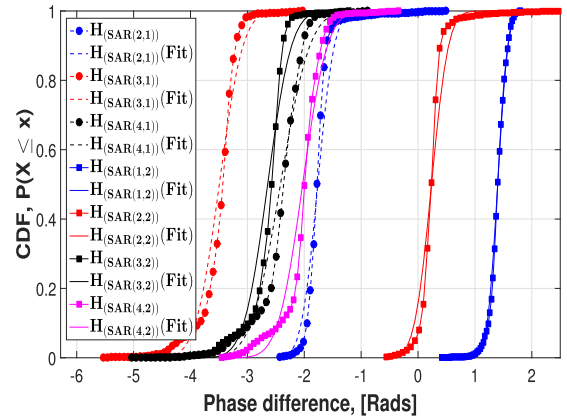

FIGURE 7. Statistical analysis of the normalized channels $\mathbf{H}_{SAR}$. The channel $\mathbf{H}_{SAR}(1, 1)$ is omitted due to normalization. Dash-dot lines & circles are used for all channels pertaining to Tx1 while solid lines & squares pertain to Tx2. All fits are Gaussian and the associated shaping parameters are tabulated in Table 4.

this work as:

$$\mathbf{B}_{42} = \begin{bmatrix} 5.9392 & 2.1938 + j4.3131 \\ 2.1938 - j4.3131 & 5.7680 \end{bmatrix}, \tag{20}$$

$$\mathbf{B}_{32} = \begin{bmatrix} 5.6119 & 1.6157 + j4.1135 \\ 1.6157 - j4.1135 & 4.6249 \end{bmatrix}, \tag{21}$$

$$\mathbf{B}_{22} = \begin{bmatrix} 2.7182 & -0.3833 + j1.9874 \\ -0.3833 - j1.9874 & 1.6818 \end{bmatrix}. \tag{22}$$

VI. RESULTS

SAR reduction and QoS at the AP are first examined while the EI is then calculated to provide long term measure of the benefit of implementing the proposed scheme. It should be stressed that all of the calculations and analysis presented throughout are based on convolving $\mathbf{X}$ with the full CIR measurements in the arrays $\widehat{\mathbf{H}}_{SAR}(\tau, i, j, t)$ and $\widehat{\mathbf{H}}_{AP}(\tau, i, j, t)$ from Section III-B except for the fact that the matrix $\mathbf{B}$, which forms part of the SAR aware design of the precoder $\mathbf{W}$, was derived as described in Section V-B and was then fixed for the various configurations $N_{Rx} \times N_{Tx}$ as in (20) - (22).

(a) Full PC.

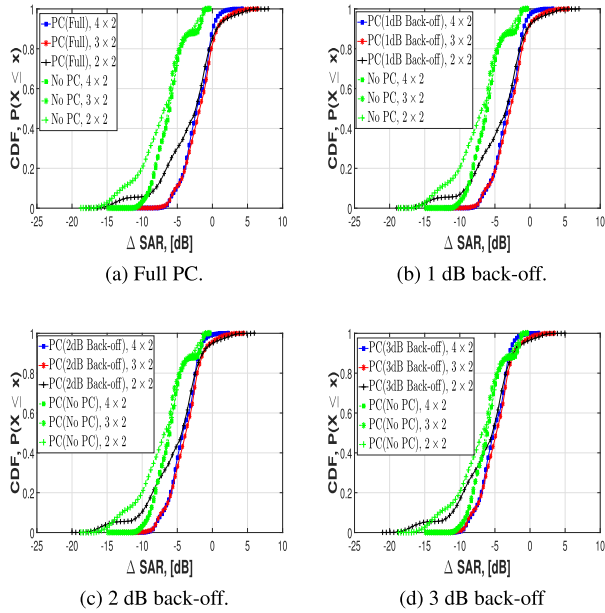(b) 1 dB back-off.

(c) 2 dB back-off.

(d) 3 dB back-off

FIGURE 9. CDFs of ∆SAR taken from aggregated calculations over all six scenarios and all three Tx pairs. Full PC, no PC and back-offs of 1 dB, 2 dB, & 3 dB are shown and in each plot the configurations $\{N_{Rx} \times N_{Tx}\} = \{4 \times 2, 3 \times 2, 2 \times 2\}$ are evaluated.
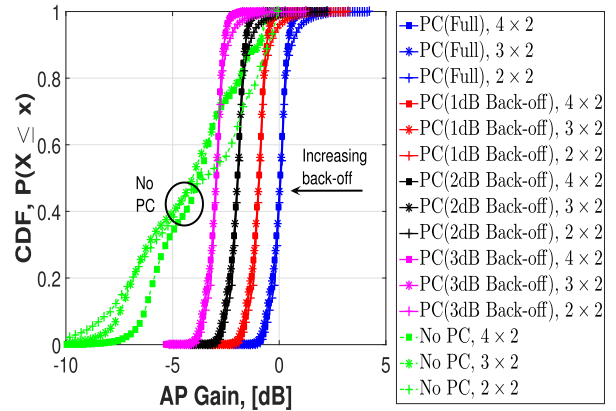

FIGURE 10. CDFs of gain at the AP taken from aggregated calculations over all six scenarios and all three Tx pairs for the different configurations of $\{N_{Rx} \times N_{Tx}\} = \{4 \times 2, 3 \times 2, 2 \times 2\}$. Full PC, no PC and back-offs of 1 dB, 2 dB, & 3 dB are shown.

relax the power control at the AP and deduce the effect of various levels of QoS sacrifice at the AP. Negative values of ∆SAR refer to reductions in SAR and it is clear that in greater than 90 % of cases, there is a significant reduction in SAR thus validating the overall approach. However careful inspection of each plot in Fig. 9 also shows that as the number of probe receivers decreases, the probability of greater levels of SAR increases. This is likely due to the fact that because there are less Rx probes, the overall channel matrix $\mathbf{H}_{SAR}$ into the chest becomes less distinct and less well-defined thus making it harder for the precoder to steer energy away from the chest and towards the AP. This analysis therefore suggests that having statistical information for at least four channels into the chest from the Tx is necessary for good performance. The QoS in terms of the gain at the AP is then examined in Fig. 10 under the same conditions. It is clear that the Rx probe configuration, i.e., 4×2, 3×2 & 2×2, matters very little at the AP as the three curves pertaining to these configurations largely sit on top of one another for each of the four back-off levels, i.e., Full PC, 1 dB, 2 dB, & 3 dB. Thus in this case, it is merely the back-off level that determined the QoS.

Finally, in the case of both Fig. 9 and Fig. 10, the effect of not implementing the PC algorithm is investigated. Clearly, significant reductions in SAR are possible but these are at the cost of an unacceptably poor levels of QoS at the AP. Furthermore, it may be observed that a back-off level of 3 dB provides SAR reduction that is comparable to the case of no PC but that is not as detrimental to the QoS at the AP.

B. BER ANALYSIS

In order to provide a more complete verification of the QoS at the AP, a full BER simulation of the system incorporating

10 MHz LTE MIMO-OFDM signal that uses SFBC signal processing stages in conjunction with the precoding, $\mathbf{W}$, and the matched filtering, $\widehat{\mathbf{W}}$, is depicted in Fig. 1. The simulation itself is an extension of the one provided in [36] and as well as incorporating the necessary additional signal processing stages, it is extended also by the inclusion of channel measurements undertaken in this work. Specifically, these measurements pertain to scenario 1 from Table 2 and for the sake of brevity will be referred to as: $\mathbf{H}_{AP}$ hereafter. The results of the analysis from it are depicted in Fig. 11. All channels are normalized according to: $\mathbb{E}\{\|\mathbf{H}\|_F^2\} = N_{Tx} \times N_{Rx}$, where $\|.\|_F$ refers to the Frobenius norm, and the modulation scheme used in each case was 4-QAM. Firstly, the performance of just the 10 MHz LTE MIMO-OFDM system is provided for two channel model types referred to as, 'AWGN', which is a very simple channel model where just added white Gaussian noise (AWGN) samples are added to the signal, and, 'PedA (WINNER)', which is channel model recommended as an effective testing channel by the WiMAX forum and is defined by the wireless world initiative new radio (WINNER) consortium in [38]. These two channel models act as a means of benchmarking the performance of $\mathbf{H}_{AP}$ and the system model proposed in this work. Also, as highlighted by the collective labeling of curves in Fig. 11, clearly the performance of all schemes pertaining to $\mathbf{H}_{AP}$ lie between the two performance extrema offered by these two channel models. As can be seen, when $\mathbf{H}_{AP}$ was implemented on its own, its performance is equivalent to that when it was implemented with precoding and full PC, thus indicating no performance loss. However, as before in Section VI-A in relation to AP gain, relaxing the PC to varying degrees, i.e., back-off, in the $\mathbf{H}_{AP}$ channel causes the QoS performance to degrade a little in a corresponding manner. However as can be appreciated from all of the analyses thus far, if small amounts of back-off, say 1-2 dB, can produce tolerably minor QoS degradation then more significant decreases in long-term exposure may be possible than in the case of full PC. This will be explored in more detail in the next Section.
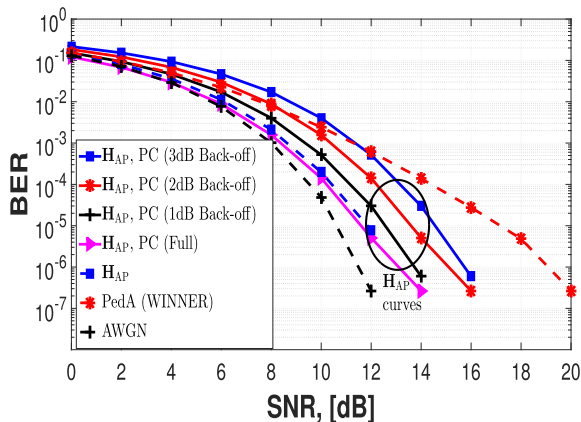
FIGURE 11. Simulations of precoding and varying degrees of PC incorporating the 10 MHz LTE MIMO OFDM signal in conjunction with 4-QAM. H_{AP} refers to channel measurements between the UT and the AP pertaining to scenario 1. The performance of AWGN and PedA channel models were included in order to benchmark the results.

C. EI REDUCTION

The exposure index (EI) is a time averaged measure of how much exposure to EM has been suffered by an individual due to a certain technology that incorporates SAR. The goal of the six-scenario measurement campaign in this work was to try to provide an impression of the long term effect of introducing this precoding and PC scheme and hence using the EI metric here is reasonable. It may be expressed as [5], [7]:

$$E = \frac{1}{T_s} \sum_{t=1}^{N_{T_s}} \left\{ \left[\frac{\text{SAR}}{P_{\text{ref}}} \right] \sum_t \left\{ \widehat{p}(T) + \sum_n \{p(t)\} \right\} \right\} l. \quad (25)$$

This metric imagines a cellular scenario where E is the uplink EI of a given user in a given cell. Similarly, $\text{SAR}/P_{\text{ref}}$ is the SAR level of the same given user referenced to a power of $P_{\text{ref}} = 1$ W. $\widehat{p}$ is the signaling power of the given user in a given sector. Similarly p is the transmit power of the given user on a given subcarrier, n, in a given sector in a timeslot, t, of length l seconds. Since T_s is the total time period under consideration, the operator $\frac{1}{T_s} \sum_{t=1}^{N_{T_s}} \{\cdot\}$ performs the time averaging. In their scheduling-based approach to SAR reduction in [5], [7], the quantity $\text{SAR}/P_{\text{ref}}$ is set to unity and focus is on developing a scheduling algorithm to reduce the term $\sum_t \left\{ \widehat{p}(T) + \sum_n \{p(t)\} \right\} l$. Careful inspection of (25) reveals that any effort to reduce the SAR will in fact scale linearly with what could be achieved using scheduling. As a result of this observation, in contrast here, make the setting $\sum_t \left\{ \widehat{p}(T) + \sum_n \{p(t)\} \right\} l = 1$ and it will be the SAR reductions $\text{SAR}/P_{\text{ref}}$ that will be applied to (25). Since there are three antenna pairs under six scenarios where in each case a total of 3000 LTE frames were evaluated with each LTE frame being transmitted over a time-period of 10 ms [31], $T_S = 3 \times 6 \times 3000 \times 10 \times 10^{-3} = 540$ s. Similarly, $N_{T_S} = 3 \times 6 \times 3000 = 54000$. Further to this in [39], the percentage EI reduction $\text{EI}_\%$ was introduced in order quantify

the effectiveness of any technology to reduce EM exposure as:

$$\text{EI}_\% = \frac{\widehat{E} - E}{E} \times 100, \quad (26)$$

where $\widehat{E}$ is the EI when the new technological solution is applied, in this case the precoding and PC algorithm, and E is the EI before the new solution was applied. In Fig. 12, the $\text{EI}_\%$ is plotted with respect back-off levels in steps of 0.5 dB from 0 to 3 dB. The three different plots correspond to the three different receive probe configurations previously mentioned. The EI is most impressive for the 4×2 configuration, which further supports the analysis of Sections VI-A that four Rx probes are necessary for good exposure reduction performance. With regard to this configuration, it is clear from Fig. 12 that the solution presented here of precoding and full PC provides a 30 % reduction in EM exposure. Furthermore, if a very small reduction in QoS at the AP is allowed, i.e., a 1.5 dB back-off, as much as 50 % reduction in EM exposure is achievable.

Table 5 provides a complete summary of the various trade-offs made here when considering antenna configuration $N_{\text{Rx}} \times N_{\text{Tx}}$ and back-off. The effects that these trade-offs have on EI reduction $\text{EI}_\%$ and QoS, in terms of median AP Gain, are provided. From careful examination of Table 5, it may be concluded firstly that QoS is largely equivalent to back-off even regardless of antenna configuration. This is not surprising but nevertheless confirms the effectiveness of the PC algorithm. Secondly, it may also be observed that while back-off may provide useful additional exposure reduction if the signal strength at the AP is reasonably high, the use of four probe antennas is recommended when developing SAR awareness for $\widehat{\mathbf{W}}$ as its results are the most impressive, particularly when there is not too much back-off. The likely reason for this is that greater decorrelation would exist between $\mathbf{H}_{\text{SAR}}$ and $\mathbf{H}_{\text{AP}}$, and hence between $\mathbf{A}$ and $\mathbf{B}$, with four Rx probe channels than with two. To test this hypothesis, observe that $\mathbf{A}$ and $\mathbf{B}$ are Hermitian and thus it possible to introduce the following metric, $d_{\mathbf{AB}}$, which is based on the correlation matrix distance metric introduced in [40]:

$$d_{\mathbf{AB}} = 1 - \frac{\text{tr}\{\mathbf{AB}\}}{\|\mathbf{A}\|_F \|\mathbf{B}\|_F}, \quad (27)$$

where $\text{tr}\{.\}$ is the trace of a matrix. $d_{\mathbf{AB}}$ varies between zero, where the two matrices $\mathbf{A}$ and $\mathbf{B}$ would be equivalent up to a scale factor and hence highly correlated, and one, where the two matrices would be maximally different from one another and hence completely decorrelated. In applying this metric, $\mathbf{A}$ is averaged based on the taking frequency domain instances of each measured CIR while $\mathbf{B}$ is based directly on (20) - (22). CDFs based on applying this metric across all scenarios and Tx pairs for a given configuration $N_{\text{Rx}} \times N_{\text{Tx}}$ are provided in Fig. 13. It is quite clear that the configuration 4×2 exhibits the maximal accumulated probability of instances of high $d_{\mathbf{AB}}$, thus supporting the aforementioned hypothesis. It should be stressed here finally that APs with

TABLE 5. Summary of trade-offs when varying the back-off and probe antenna configuration $N_{Rx} \times N_{Tx}$ and and their effects on percentage EI reduction $EI_\%$ and the QoS as measured by the median AP Gain.

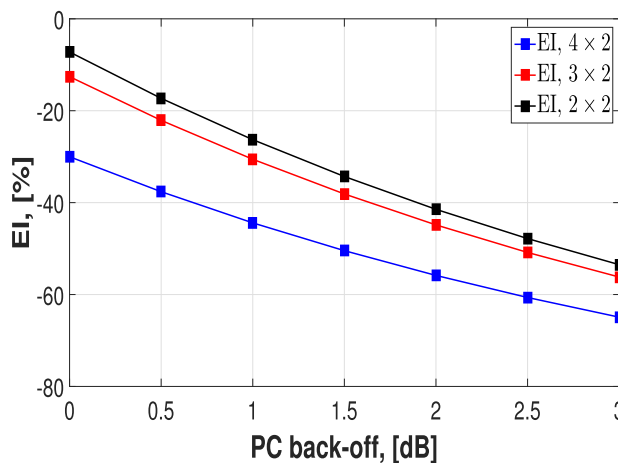| Back-off	$N_{Rx} \times N_{Tx}$	$EI_\%$	QoS
0 dB	4×2	-30.01 %	0.05 dB
1 dB	4×2	-44.40 %	-0.95 dB
2 dB	4×2	-55.84 %	-1.94 dB
3 dB	4×2	-64.92 %	-2.94 dB
0 dB	3×2	-12.59 %	0.01 dB
1 dB	3×2	-30.57 %	-0.99 dB
2 dB	3×2	-44.85 %	-1.99 dB
3 dB	3×2	-56.20 %	-2.98 dB
0 dB	2×2	-7.22 %	0.01 dB
1 dB	2×2	-26.30 %	-0.98 dB
2 dB	2×2	-41.46 %	-1.98 dB
3 dB	2×2	-53.50 %	-2.98 dB

FIGURE 12. The % EI reduction as a function of power back-off for the different configurations of $\{N_{Rx} \times N_{Tx}\} = \{4 \times 2, 3 \times 2, 2 \times 2\}$. 0 dB corresponds to full PC.

higher antenna spacings than the one here may also improve performance due to the fact that these greater spacing would introduce more decorrelation in the channel matrix of $\mathbf{H}_{AP}$.

D. COMPARISON WITH OTHER WORKS

Table 6 compares other relevant signal processing approaches under percentage EI reduction, complexity, number of independent transmit streams N_{Str} permitted and whether or not perfect transmit CSI is required. A 50-60 % EI reduction was achievable in [20] through Rx beamforming and although this did not require any additional complexity because the maximum likelihood receiver employed could simply be redesigned, it could not support multi-stream transmission. Similarly, the SAR codes approach in [23], [24], while achieving 55 % without significant additional complexity overhead, did not achieve truly independent multi-stream transmission. It also had other serious issues (detailed in Section I) that were namely that it was impractical for use in OFDM systems and that the modulation-symbol design could lead to impractical modulation alphabets. Eigenmode
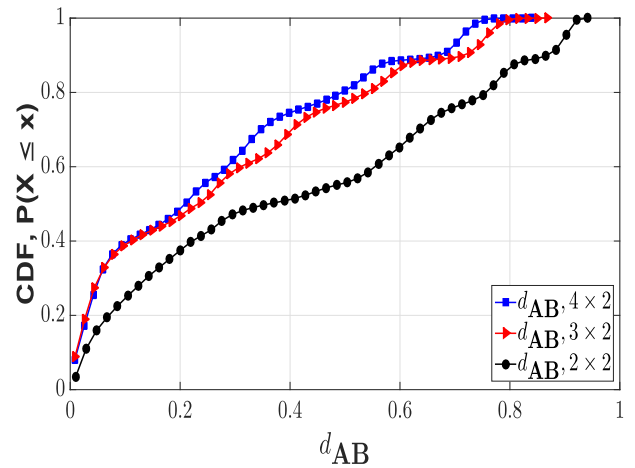

FIGURE 13. CDFs of calculations of d_{AB} across all scenarios and Tx pairs as a function of each probe configuration $\{N_{Rx} \times N_{Tx}\} = \{4 \times 2, 3 \times 2, 2 \times 2\}$. The configuration 4×2 exhibits the maximal accumulated probability of high values for d_{AB}.

TABLE 6. Comparison with other works under percentage EI reduction $EI_\%$, additional complexity, number of independent transmit streams N_{Str} permitted and whether or not perfect transmit CSI is required.

Approach	$EI_\%$	Complexity	N_{Str}	Tx CSI
Rx beamforming [20]	50-60%	0	1	No
Eigenmode waterfilling [21]	27-90%	$\mathcal{O}(N^3) + \alpha$	N_{Tx}	Yes
SAR codes [23] [24]	55%	0	$< N_{Tx}$	No
Emission aware scheduling [5] [7]	100-fold	100-fold	N_{Tx}	Yes
Precoding & PC	30-50%	$\mathcal{O}(N^3)$	N_{Tx}	No

waterfilling requires a cubed polynomially increasing complexity and like the approach offered by this work, the system model pertained to a narrowband channel. Also, since a waterfilling algorithm is employed, an additional amount of complexity, referred to hereafter as α simply because the authors in [21] were not explicit about how much it should be, will also be required. As well as this, waterfilling also necessitates perfect Tx CSI. Since the emission aware scheduling in [5], [7] is a system level technology, it must be compared directly with another appropriate system level approach that does not consider exposure reduction. Fortunately in Fig. 8 in [5], this was offered where a 100-fold increase in complexity is required to offer a 100-fold decrease in exposure. While the exposure reduction is impressive, the increased complexity is significant. Also, while this system can facilitate full multi-stream transmission, this system also requires perfect TX CSI.

Although the precoding & PC approach suggested in this work also requires a cubed polynomially increasing complexity because eigenvectors must be calculated, it does not require the additional complexity α associated with the nature of any waterfilling algorithm being employed and which is likely to be significant. Also, since only one eigenvector per transmission block is required with no waterfilling, perfect Tx

CSI is not required and furthermore complete multi-stream transmission may be facilitated. Thus, the proposed approach offers a reasonable trade-off between complexity and EI reduction while also offering truly independent multi-stream transmission for MIMO systems without the need for perfect Tx CSI, which is often impractical to obtain.

VII. CONCLUSION

In this work, a novel precoding and PC algorithm was developed in order to reduce EM exposure while maintaining adequate levels of QoS at the AP for the use-case of an indoor laptop. The practical applications of this approach are to allow for an increase in Tx power while maintaining SAR compliance or to reduce the more long term exposure of the user. Unlike other related approaches in literature, this novel scheme allows for true MIMO multi-stream transmission. Furthermore, the analysis also shows that the approach proposed here would scale linearly with other EMF exposure reduction methods and as such would act as a complimentary solution. The precoder was designed by analyzing the first order statistics of the MIMO channel between a laptop UT and user's body and in a practical implementation setting, such an analysis could be repeated by a manufacturer as it is likely to be strongly hardware-influenced. Further to this, near-field SAR models that appear in literature for smartphone channels were examined for their applicability to this far-field use-case. Their compatibility was confirmed when they were seen to behave sinusoidally with respect to a phase-offset angle, which was something that had not been clarified for far-field channels before. When the novel precoding and PC approach developed in this work was applied to a 10 MHz LTE MIMO-OFDM signal, a 30 % reduction in EM exposure was observed. Furthermore, if a small degree of reduction in QoS could be tolerated at the AP, as much as 50 % reduction in EM exposure could then be obtained.

REFERENCES

[1] (May 2011). *IARC Classifies Radiofrequency Electromagnetic Fields as Possibly Carcinogenic to Humans*. Accessed: Nov. 2020. [Online]. Available: https://www.iarc.fr/wp-content/uploads/2018/07/pr208_E.pdf

[2] N. D. Volkow, D. Tomasi, G.-J. Wang, P. Vaska, J. S. Fowler, F. Telang, D. Alexoff, J. Logan, and C. Wong, "Effects of cell phone radiofrequency signal exposure on brain glucose metabolism," *J. Amer. Med. Assoc.*, vol. 305, no. 8, pp. 808–813, Feb. 2011.

[3] (Dec. 2016). FCC. *Electronic Code of Federal Regulations*. Accessed: Nov. 2020. [Online]. Available: http://www.ecfr.gov/cgi-bin/text-idx?c=ecfr&tpl=/ecfrbrowse/Title47/47c%frv1_02.tpl

[4] (Jan. 1995). CENELEC. *Human Exposure to Electromagnetic Fields: High-Frequency (10 KHz–300 GHz)*. Accessed: Nov. 2020. [Online]. Available: https://www.who.int/peh-emf/publications/facts/intermediatefrequencies_%infosheet.pdf

[5] Y. A. Sambo, F. Heliot, and M. A. Imran, "Electromagnetic emission-aware scheduling for the uplink of multicell OFDM wireless systems," *IEEE Trans. Veh. Technol.*, vol. 66, no. 9, pp. 8212–8222, Sep. 2017.

[6] M. A. Jamshed, F. Heliot, and T. W. C. Brown, "A survey on electromagnetic risk assessment and evaluation mechanism for future wireless communication systems," *IEEE J. Electromagn., RF Microw. Med. Biol.*, vol. 4, no. 1, pp. 24–36, Mar. 2020.

[7] Y. A. Sambo, M. Al-Imari, F. Heliot, and M. A. Imran, "Electromagnetic emission-aware schedulers for the uplink of OFDM wireless communication systems," *IEEE Trans. Veh. Technol.*, vol. 66, no. 2, pp. 1313–1323, Feb. 2017.

[8] H. B. A. Sidi, Z. Altman, and A. Tall, "Self-optimizing mechanisms for EMF reduction in heterogeneous networks," in *Proc. 12th Int. Symp. Model. Optim. Mobile, Ad Hoc, Wireless Netw. (WiOpt)*, May 2014, pp. 341–348.

[9] K.-C. Chim and R. D. Murch, "Investigating the effect of smart antenna on SAR," in *Proc. IEEE Antennas Propag. Soc. Int. Symp.*, Jun. 2002, pp. 432–435.

[10] K.-C. Chim, K. C. L. Chan, and R. D. Murch, "Investigating the impact of smart antennas on SAR," *IEEE Trans. Antennas Propag.*, vol. 52, no. 5, pp. 1370–1374, May 2004.

[11] K. W. Kim and Y. Rahmat-Samii, "Handset antennas and humans at Ka-band: The importance of directional antennas," *IEEE Trans. Antennas Propag.*, vol. 46, no. 6, pp. 949–950, Jun. 1998.

[12] A. Iqbal, O. A. Saraereh, A. W. Ahmad, and S. Bashir, "Mutual coupling reduction using F-shaped stubs in UWB-MIMO antenna," *IEEE Access*, vol. 6, pp. 2755–2759, 2018.

[13] M. Alibakhshikenari, B. S. Virdee, C. H. See, R. A. Abd-Alhameed, F. Falcone, and E. Limiti, "Surface wave reduction in antenna arrays using metasurface inclusion for MIMO and SAR systems," *Radio Sci.*, vol. 54, no. 11, pp. 1067–1075, Nov. 2019.

[14] M. Alibakhshikenari, B. S. Virdee, P. Shukla, C. H. See, R. Abd-Alhameed, M. Khalily, F. Falcone, and E. Limiti, "Interaction between closely packed array antenna elements using meta-surface for applications such as MIMO systems and synthetic aperture radars," *Radio Sci.*, vol. 53, no. 11, pp. 1368–1381, Nov. 2018.

[15] A. Iqbal, J. J. Tiang, C. K. Kee, and B. M. Lee, "Tunable substrate integrated waveguide diplexer with high isolation and wide stopband," *IEEE Microw. Wireless Compon. Lett.*, vol. 29, no. 7, pp. 456–458, Jul. 2019.

[16] M. M. Shirkolaei, "Wideband linear microstrip array antenna with high efficiency and low side lobe level," *Int. J. RF Microw. Comput.-Aided Eng.*, vol. 30, no. 11, Nov. 2020, Art. no. e22412.

[17] L. Zheng and D. N. C. Tse, "Diversity and multiplexing: A fundamental tradeoff in multiple-antenna channels," *IEEE Trans. Inf. Theory*, vol. 49, no. 5, pp. 1073–1096, May 2003.

[18] F. Haider, C.-X. Wang, B. Ai, H. Haas, and E. Hepsaydir, "Spectral/energy efficiency tradeoff of cellular systems with mobile femtocell deployment," *IEEE Trans. Veh. Technol.*, vol. 65, no. 5, pp. 3389–3400, May 2016.

[19] F. Haider, C. X. Wang, H. Haas, E. Hepsaydir, X. Ge, and D. Yuan, "Spectral and energy efficiency analysis for cognitive radio networks," *IEEE Trans. Wireless Commun.*, vol. 14, no. 6, pp. 2969–2980, Jun. 2015.

[20] B. M. Hochwald and D. J. Love, "Minimizing exposure to electromagnetic radiation in portable devices," in *Proc. Inf. Theory Appl. Workshop (ITA)*, Feb. 2012, pp. 255–261.

[21] D. Ying, D. J. Love, and B. M. Hochwald, "Closed-loop precoding and capacity analysis for multiple-antenna wireless systems with user radiation exposure constraints," *IEEE Trans. Wireless Commun.*, vol. 14, no. 10, pp. 5859–5870, Oct. 2015.

[22] J. Xiong, L. You, D. W. K. Ng, W. Wang, and X. Gao, "Energy-efficient precoding in electromagnetic exposure-constrained uplink multiuser MIMO," *IEEE Trans. Veh. Technol.*, vol. 70, no. 7, pp. 7226–7231, Jul. 2021.

[23] B. M. Hochwald, D. J. Love, S. Yan, and J. Jin, "SAR codes," in *Proc. Inf. Theory Appl. Workshop (ITA)*, Feb. 2013, pp. 1–9.

[24] B. M. Hochwald, D. J. Love, S. Yan, P. Fay, and J.-M. Jin, "Incorporating specific absorption rate constraints into wireless signal design," *IEEE Commun. Mag.*, vol. 52, no. 9, pp. 126–133, Sep. 2014.

[25] M. Sadek, A. Tarighat, and A. H. Sayed, "A leakage-based precoding scheme for downlink multi-user MIMO channels," *IEEE Trans. Wireless Commun.*, vol. 6, no. 5, pp. 1711–1721, May 2007.

[26] C. B. Peel, B. M. Hochwald, and A. L. Swindlehurst, "A vector-perturbation technique for near-capacity multiantenna multiuser communication—Part I: Channel inversion and regularization," *IEEE Trans. Commun.*, vol. 53, no. 1, pp. 195–202, Jan. 2005.

[27] B. M. Hochwald, C. B. Peel, and A. L. Swindlehurst, "A vector-perturbation technique for near-capacity multiantenna multiuser communication - Part II: Perturbation," *IEEE Trans. Communs.*, vol. 53, no. 3, p. 203, Mar. 2005.

[28] MobileMark. *Surface Mount Micro WiFi, WiMAX & 4.9 Public Safety*. Accessed: Nov. 2020. [Online]. Available: https://docs.rs-online.com/d41c/0900766b80f140e8.pdf

[29] M. C. Gosselin, G. Vermeeren, S. Kühn, V. Kellerman, S. Benkler, T. M. I. Uusitupa, W. Joseph, A. Gati, J. Wiart, F. J. C. Meyer, L. Martens, T. Nojima, T. Hikage, Q. Balzano, A. Christ, and N. Kuster, "Estimation formulas for the specific absorption rate in humans exposed to base-station antennas," *IEEE Trans. Electromagn. Compat.*, vol. 53, no. 4, pp. 909–922, Nov. 2011.

[30] *Human Exposure to Radio-Frequency Fields from Handheld and Body-Mounted Wireless Communication Devices—Human Models, Instrumentation, and Procedures, Part 2: Procedure to Determine the Specific Absorption Rate (SAR) for Mobile Wireless Communication Devices Used in Close Proximity to the Human Body (Frequency Range of 30 MHz to 6 GHz)*, Cham, Switzerland, International Electrotechnical Commission (IEC), IEC Technical Committee, 2007. [Online]. Available: https://standards.iteh.ai/catalog/standards/clc/02edebeb-aeb3-4126-8bac-f30236c6ac20/en-62209-2-2010-a1-2019

[31] S. Sesia, I. Toufik, and M. Baker, *LTE—The UMTS Long Term Evolution: From Theory to Practice*, 2nd ed. Hoboken, NJ, USA: Wiley, 2011.

[32] R. C. Browning, E. A. Baker, J. A. Herron, and R. Kram, "Effects of obesity and sex on the energetic cost and preferred speed of walking," *J. Appl. Physiol.*, vol. 100, no. 2, pp. 390–398, Feb. 2006.

[33] Y. Wang, W.-J. Lu, and H.-B. Zhu, "Propagation characteristics of the LTE indoor radio channel with persons at 2.6 GHz," *IEEE Antennas Wireless Propag. Lett.*, vol. 12, pp. 991–994, 2013.

[34] A. K. Salkintzis and P. T. Mathiopoulos, "On the combining of multipath signals in narrowband Rayleigh fading channels," *IEEE Trans. Broadcast.*, vol. 45, no. 2, pp. 192–195, Jun. 1999.

[35] T. H. Nguyen, T. V. Chien, H. Q. Ngo, X. N. Tran, and E. Bjornson, "Pilot assignment for joint uplink-downlink spectral efficiency enhancement in massive MIMO systems with spatial correlation," *IEEE Trans. Veh. Technol.*, vol. 70, no. 8, pp. 8292–8297, Aug. 2021.

[36] C. Mehlführer, J. C. Ikuno, M. Šimko, S. Schwarz, M. Wrulich, and M. Rupp, "The Vienna LTE simulators–Enabling reproducibility in wireless communications research," *EURASIP J. Adv. Signal Process.*, vol. 2011, no. 1, pp. 1–14, Jul. 2011.

[37] S. Park, A. Q. Truong, and T. H. Nguyen, "Power control for sum spectral efficiency optimization in MIMO-NOMA systems with linear beamforming," *IEEE Access*, vol. 7, pp. 10593–10605, 2019.

[38] P. Kyosti, J. Meinila, L. Hentila, X. Zhao, and T. Jamsa, "ST-4-027756 WINNER II D1.1.2 V1.2, WINNER II channel models, part 1," EBITG, TUI, UOULU, CU/CRC, NOKIA, Tech. Rep., 2014. [Online]. Available: http://www.ero.dk/93F2FC5C-0C4B-4E44-8931-00A5B05A331B?frames=no&

[39] N. Varsier, Y. Huang, A. Krayni, A. Hadjem, J. Wiart, G. Vermeeren, D. Plets, W. Joseph, L. Martens, Y. Corre, C. Oliveira, D. Sao, L. Correia, M. Koprivica, M. Popović, E. Kocan, M. Pejanovic-Djurisic, P. Wiedemann, and F. Freudenstein, "D2.6: Global wireless exposure metric definition," LEXNET Consortium, Tech. Rep., Nov. 2014. [Online]. Available: https://cordis.europa.eu/docs/projects/cnect/3/318273/080/deliverables/001-D21Currentexposuremetricsv40Ares20142440252.pdf

[40] M. Herdin, N. Czink, H. Ozcelik, and E. Bonek, "Correlation matrix distance, a meaningful measure for evaluation of non-stationary MIMO channels," in *Proc. IEEE 61st Veh. Technol. Conf.*, May 2005, pp. 136–140.

PAT CHAMBERS (Member, IEEE) received the B.Sc. degree in physics & physics technology and the Ph.D. degree in engineering from Technological University Dublin, Ireland, in 2002 and 2008, respectively, as well as the M.A. degree in teaching & learning from the Institute of Technology Carlow, Ireland, in 2021.

He has worked on various EU and worldwide projects and was part of the team that demonstrated the first over-the-air implementation of spatial modulation. His other research interests include multiple antenna technologies for exposure reduction and spectrum sensing for cognitive radio. Having previously been a Lecturer in electronic engineering at Heriot-Watt University, Edinburgh, U.K. He is now a Visiting Lecturer with Southwest University, Chongqing, China, on their global immersion program and is also a full-time Lecturer with the Institute of Technology Carlow.

TIM W. C. BROWN (Member, IEEE) received the B.Eng. degree in electronic engineering from the University of Surrey, U.K., in 1999, and the Ph.D. degree in antenna diversity for mobile terminals from the Centre for Communication Systems Research (CCSR) (Now named the Institute for Communications Systems), in 2004.

Since completing his postdoctoral research, he has continued his research interests in antennas, propagation, and radio frequency (RF) engineering. This has included postdoctoral research with Aalborg University, Denmark, from 2004 to 2006, and his present post as an Associate Professor in RF, antennas and propagation with the University of Surrey. His research interests include multi antenna technologies both for capacity enhancement but also ultra low exposure devices and wireless networks.

● ● ●